clean technologies

MDPI

Article

The Potential to Produce Bio-Based Ammonia Adsorbents from Lignin-Rich Residues

Daniel Chernick, Valerie Dupont * and Andrew B. Ross

School of Chemical and Process Engineering, University of Leeds, Woodhouse Lane, Leeds LS2 9JT, UK; pmdsc@leeds.ac.uk (D.C.); a.b.ross@leeds.ac.uk (A.B.R.)
* Correspondence: v.dupont@leeds.ac.uk

Abstract: The ammonia adsorption capacity of lignin-rich biomass solids was tested for the first time at low partial pressures (<1.5 kPa) and 20 °C. The biomass samples included untreated tree barks, husks, and peats, as well as the biochars produced by their slow pyrolysis. Proximate and ultimate analyses, lignin content, and metal content are also presented. The untreated biosolids had higher VM/FC ratios, molar H/C, and O/C than the treated biosolids (biochars and treated biochars). A novel methodology is described for the safe generation of gaseous ammonia at predictable low partial pressures from tabletop-scale batch reaction experiments of NaOH with $(NH_4)_2SO_4$ in aqueous solution, leading to the determination of ammonia adsorption capacities from low-cost experiments. Statistically significantly larger NH_3 adsorption capacities were obtained for the untreated biosolids than for their biochars ($p < 0.001$). In contrast, the biochars were found to be poor NH_3 adsorbers without further treatment. The NH_3 adsorption capacities from this study's biosolids were compared with those of common adsorbent types in the same conditions using the existing literature through equilibrium model interpolation (Dubinin–Astakhov, Toth, and Freundlich) or cubic spline fit from graphical isotherms. Controls consisting of commercially sourced activated carbons (AC) had low adsorption capacities, close to those derived from the literature in the same conditions for similar materials, confirming the methodology's robustness. The untreated biosolids' NH_3 adsorption capacities were in the same range as those reported for silica, gamma-alumina, and some of the treated or doped ACs. They also performed better than the undoped, untreated ACs. The work suggests lignin-rich untreated biosolids such as barks and peats are competent low-cost ammonia adsorbents.

Keywords: ammonia; adsorption; tree bark; peat; biochar; Dubinin–Astakhov; Toth; Freundlich

Academic Editors: Alírio E. Rodrigues and Beatriz Valle

Received: 14 January 2025
Revised: 28 March 2025
Accepted: 3 April 2025
Published: 5 April 2025

Citation: Chernick, D.; Dupont, V.; Ross, A.B. The Potential to Produce Bio-Based Ammonia Adsorbents from Lignin-Rich Residues. *Clean Technol.* **2025**, *7*, 30. https://doi.org/10.3390/cleantechnol7020030

1. Introduction

Ammonia (NH_3) is a compound that is present in nature [1] and is one of the most industrially produced chemicals in the world [2]. Ammonia production is currently the largest CO_2 emitting chemical industry process [3]. The greatest consumption of ammonia (≈80 vol%) is in the production of fertilisers including ammonium nitrate, ammonium hydrogen phosphate, ammonium sulphate, and urea [4,5]. Around 90% of global emissions of ammonia arise from the agriculture sector [6], predominantly from NH_3-based fertilisers and animal manure [7].

Ammonia, in excess, poses a threat to human health and leads to water body eutrophication [8] and environmental pollution. Whilst gaseous ammonia is present in the atmosphere [9], it can react chemically with aerosols and acidic gases that are already

there, contributing to greater levels of aerosol formation [10] and other secondary pollutants [11]. Aqueous ammonium is commonly found in high levels in wastewaters and agricultural run-off streams. Due to strict discharge regulations, many ammonia-rich wastewaters are prevented from being discharged or re-used [12]. Through the removal of ammonia, wastewaters can be returned to the water source for re-use or are used further for non-potable purposes (irrigation, vehicle washing, agriculture, or firefighting) [13]. The recycling of gaseous ammonia or aqueous ammonium from biowaste and biomass streams can help to reduce the impact of ammonia emissions and the net production of energy-intensive products.

Gaseous ammonia can be captured through the use of adsorbents. These are materials that perform physical and/or chemical adsorption. Desirable adsorbents have high thermal stability and strong mechanical properties, are rich in functional groups, and have high pore volumes [14,15]. Common adsorbents can be inorganic (alumina, silica, zeolites) [16] or organic (activated carbons, coal ash). Inorganic adsorbents are more frequently used than organic adsorbents as they are produced and commercialised at larger scales. They also carry higher environmental impacts as their production is energy-intensive mainly due to refining [17] or prolonged calcination times [18,19]. In addition, inorganic adsorbents such as zeolites perform well as adsorbents because of their high levels of chemical functionality and large surface areas [20]. The adsorption potential of organic adsorbents like biomass has been improved in the literature by a variety of activation methods [21]. These have included chemical activation (with acids, alkalis, and steam) [22–24], physical activation (hydrothermal carbonisation and pyrolysis) [25,26], and metals incorporation [27]. Chemical activation is typically performed to form a coating on the surface of the adsorbent to increase its chemical functionality [28], whilst physical activation is performed to open the pores on the surface of the adsorbent and thereby increase its surface area [29]. The incorporation of metals such as Fe, Zn, Zr, and Ni into activated carbons has been shown to improve adsorption capacity of organic compounds and heavy metals through the enhancement of surface area, pore volume, and O content [30]. However, this has been examined less where ammonia was the sorbate of interest [31].

It has been posited previously [32] that for an adsorbent to have a high adsorption capacity, it requires a large surface area and high chemical functionality. Activated carbons, commonly from pyrolysed biomass, are likely to have a larger surface area than untreated biomass but at the cost of reduced chemical functionality. Takaya et al. [32] compared the ammonia adsorption capacities of chars from pyrolysed biomass (biochars) and hydrothermally carbonised biomass (hydrochars). The hydrochars were seen to have greater adsorption capacities than the biochars, despite maintaining a low surface area, but featured higher chemical functionality. The high chemical functionality is expected to be due to the complex structure of biomass, in particular where the lignin content is higher. This is because the other main components of lignocellulosic biomass (cellulose and hemicellulose) thermally degrade at lower temperatures than lignin during hydrothermal carbonisation.

Untreated tree barks are known to be high in lignin [33], and their use as adsorbents is not as energy intensive as the production of hydrochars, biochars, or inorganic adsorbents. In addition, the lignin contents of tree barks are commonly higher than in the wood from the same tree [34].

Tree barks are forestry residues that are generated either from its harvesting directly from a live tree, such as with cork oaks [35], or after the timber has been debarked, such as at sawmills. There is estimated to be about 300–400 million m^3 of bark generated each year from lumbered roundwoods [36]. However, only a small proportion of bark is commercially utilised. Most of its utilisation is in low-value applications, either as a source of energy through incineration or as mulch for agricultural land.

In this work, biomass solids were tested for their adsorption capacity (both untreated and as biochars produced by slow pyrolysis of the raw biomass) for the first time. The statistical significance of the effects of the treatments were examined, and the adsorption capacities from this study were compared to those of common organic and inorganic ammonia adsorbents at the same NH_3 partial pressures and temperature as in in our experiments to highlight the potential valorisation of the residues.

2. Materials and Methods

2.1. Materials

Coconut husk (CH) was obtained by de-shelling whole coconuts purchased in Leeds, UK at a local supermarket.

Bark-free holm oak wood (oak) and its biochar (produced at 450 °C) (Oakbc450) were provided by the Fertiplus Consortium (Grant Agreement N°: 289853) (Malaga, Spain, Proininso SA), co-funded by the European Commission, Directorate General for Research and Innovation, within the 7th Framework Programme of RTD, Theme 2—Biotechnologies, Agriculture, and Food. The pyrolysis to produce the biochar was performed in a mono retort reactor for 60 min in the absence of oxygen.

Two types of peat were analysed. An Irish sphagnum moss peat ('PeatMoss'), and a peat turf ('PeatSEPO'). Two different types of commercial activated carbons were tested for their ammonia adsorption potential (Buchs, Switzerland, Sigma-Aldrich). These were a NORIT RO 3515 (NORIT-AC) and activated charcoal (SIGMA-AC).

Five species of tree barks (noble fir—NF, Douglas-fir—DF, European silver fir—ESF, grand fir—GF, and Nootka cypress—NC) were provided by Abbey Timber (Scottish Borders, UK). The following abbreviations are used in the results tables: 'Raw' refers to an untreated individual tree residue, 'bc' refers to the biochar produced by slow pyrolysis of an individual tree residue, 'HW' refers to biochar pretreated with hot water prior to the NH_3 adsorption experiment, and 'AC' refers to activated carbon.

2.2. Methods

2.2.1. Slow Pyrolysis

The tree barks underwent slow pyrolysis in a vertical mode fixed-bed batch reactor at laboratory scale at 450 °C, which was held for 1 h. A nitrogen flow of 50 mL/min (to create an inert atmosphere) was maintained for 10 min prior to the heater being turned on and until the sample had been cooled to under 200 °C. A more detailed description of the pyrolysis reactor is described elsewhere [37].

2.2.2. Proximate Analysis

The proximate analysis of the biosolids, prior to the adsorption experiments, were determined by thermo-gravimetric analysis (TGA/DSC 1, Mettler Toledo GmbH, Greifensee, Switzerland). All measurements were performed in duplicate, with the mean values being reported. The heating profile used on the TGA consisted of the sample initially being heated from room temperature to 120 °C in nitrogen, which was held for 10 min. Then, the sample was heated to 900 °C and held for 30 min. Samples were analysed in duplicate. After this time, the gas was switched to air to combust the sample and produce ash. Error values were calculated by deviation from the mean. The balance used for this analysis had an error of ± 0.005 mg.

2.2.3. Lignin Content Determination

The Gerhardt Fibrecap system (as described by Fettweis and Kuhl [38]) was used to determine the neutral detergent fibre (NDF, STM 016), acid detergent fibre (ADF, STM 017),

and acid detergent lignin (ADL) [39]. First, 1 ± 0.005 g of the sample (m_{sample}) was weighed into a pre-weighed fibrebag ($m_{fibrebag}$) surrounding a pre-weighed glass spacer (m_{blank}). The soluble content is removed using a heated neutral detergent solution, followed by removal of the hemicellulose using an acid detergent step. The cellulose content is then removed using a 72% H_2SO_4 solution. Following carbohydrate removal, the acid detergent lignin (ADL) is isolated. The final lignin content is determined by ashing the ADL, as described in Equation (1).

$$\%\text{Lignin} = 100 \times \frac{(m_{ADL} - m_{fibrebag} - m_{ash}) - m_{blank}}{m_{sample}} \quad (1)$$

Samples were analysed in duplicate. Error values were calculated by deviation from the mean.

2.2.4. Metals Content

Atomic absorption spectroscopy was used to determine the calcium (Ca), potassium (K), sodium (Na), magnesium (Mg), aluminium (Al), and iron (Fe) content in the feedstocks. First, 0.2 g of the untreated biosolids were digested in duplicate in 10 wt% nitric acid solution. The solution was then analysed by flame atomic absorption spectroscopy (Model: 240FS AA, Agilent, CA, USA) on each of the digested duplicates. Error values were calculated by deviation from the mean. The balance used for this analysis had an error of ±0.005 g.

2.2.5. Ammonia Adsorption from Tabletop-Scale Reaction Experiments of NaOH with $(NH_4)_2SO_4$ in Aqueous Solution

The novel methodology presented in this work with the aim of generating adsorption isotherms at low partial pressures from low-cost, safe, tabletop-scale batch reaction experiments consist of four steps, represented in Figure 1. Step 1 is setting up the gaseous ammonia generation in a closed vessel. This part of the methodology followed the approach described by Takaya et al. [32]. The remaining steps are desk-based. Step 2 is the derivation of adsorption capacity using the N wt% contents in the samples pre- and post-adsorption, and Step 3 is the calculation of the partial pressure of ammonia generated by the batch reaction experiments of NaOH with $(NH_4)_2SO_4$ in aqueous solution.

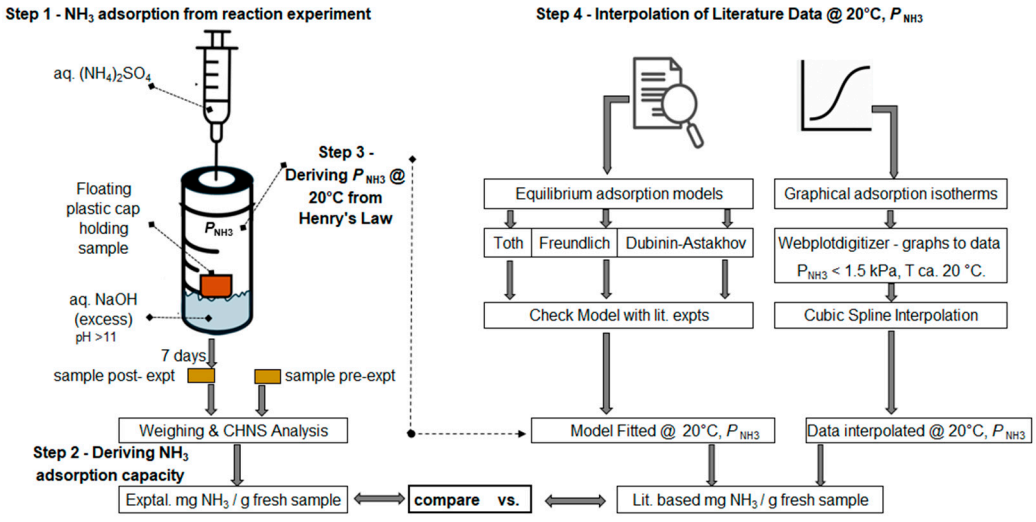

Figure 1. Graphical scheme of the methodology of ammonia adsorption from tabletop batch reaction experiments of NaOH with $(NH_4)_2SO_4$ in aqueous solution.

The fourth (final) step is the derivation of literature-based adsorption capacities of NH_3 adsorbents at the same P_{NH3} and adsorption temperature as in the experiments to enable a direct comparison with that derived in Step 2. Together, these steps represent a novel and essential combined approach that provides means of generating adsorption isotherm data and compare it with adsorption capacities reported in the literature.

Steps 1–4 are summarised in schematic form in Figure 1.

The following section describes the procedures followed in Step 1 of the methodology. The ammonia adsorption capacity was tested in a batch set-up. A known concentration and volume of aqueous sodium hydroxide (according to Table 1) was added to a 250 mL volume Duran bottle. Then, approximately 0.3 g of solid sample was added to an open vessel using an inverted plastic cap, which was then suspended inside the bottle on the NaOH solution so that it would float.

Table 1. Concentrations and volumes of ammonia adsorptions.

Experiment	1	2	3
NaOH Concentration and Volume	0.1 mol L^{-1}, 60 mL	1 mol L^{-1}, 60 mL	3 mol L^{-1}, 60 mL
$(NH_4)_2SO_4$ Concentration and Volume	0.05 mol L^{-1}, 25 mL	0.5 mol L^{-1}, 25 mL	1.76 mol L^{-1}, 25 mL
Theoretical yield of ammonia produced	43 mg	430 mg	1500 mg
Sulphuric Acid Concentration and Volume	0.05 mol L^{-1}, 30 mL	0.5 mol L^{-1}, 30 mL	1.76 mol L^{-1}, 30 mL

The Duran bottle was then closed with a tightly fitted lid with a septum to achieve a closed atmosphere. Following this, a known concentration of aqueous ammonium sulphate ($(NH_4)_2SO_4$) solution was injected into the bottle. The reaction between the NaOH and $(NH_4)_2SO_4$ produced gaseous ammonia by the following chemical reaction:

$$2\ NaOH\ (aq) + (NH_4)_2SO_4\ (aq) \rightarrow Na_2SO_4\ (aq) + 2H_2O\ (l) + 2NH_3(g) \quad (2)$$

The ammonia sorption tests were run at three different concentrations of reagents (Table 1) in duplicate, so that a known amount of gaseous NH_3 was produced. After 7 days, a known volume and concentration of aqueous sulphuric acid (in excess relative to the $(NH_4)_2SO_4$ moles) was injected into the Duran bottles to end the reaction. After 12 h, the sample vessels were removed from the Duran bottles and their contents analysed by elemental analysis.

The experiments are henceforth labelled 0.05 mol L^{-1}, 0.5 mol L^{-1}, and 1.8 mol L^{-1} to represent the $(NH_4)_2SO_4$ concentration in the $(NH_4)_2SO_4$ aqueous solution.

2.2.6. Elemental Analysis and Derivation of NH_3 Adsorption Capacity

This section describes the principles behind Step 2 of the methodology. The nitrogen mass percent contents in the samples pre- and post-NH_3 adsorption experiment (henceforth termed '$\%N_f$' and '$\%N_S$', for 'fresh' and 'spent' samples, respectively) were analysed in duplicate using an elemental analyser (Flash 2000, Thermo Scientific, Waltham, MA, USA). The instrument was calibrated and checked using calibration standards and certified biomass reference materials (Elemental Microanalysis, Devon, UK). Error values were calculated by standard deviation. As the nitrogen content measured by elemental analysis recorded the N in a spent adsorbent, '$\%N_S$', a conversion to obtain adsorption capacity

on mass of fresh adsorbent basis was required $\left(\frac{m_{NH3}}{m_f}\right)$ for comparison with adsorption isotherm data from the literature. Equations (3)–(9) describe this conversion process.

The mass of the spent adsorbent (m_s) is the sum of the fresh adsorbent (m_f) and of the ammonia adsorbed during the experiment (m_{NH3}). In Equation (3), W_{NH3} and W_N are the molar masses of NH_3 (17.04 g mol^{-1}) and N (14.01 g mol^{-1}), respectively, γ is defined as the ratio between these two molar masses, and m_N is the mass of N in the adsorbed ammonia obtained from Equation (3).

$$m_s = m_f + m_{NH3} = m_f + \frac{W_{NH3}}{W_N} m_N = m_f + \gamma m_N \quad (3)$$

$\%N_s$ is related to m_{Nf}, the mass of N in the fresh adsorbent; m_N and m_S are according to Equation (4).

$$\%N_S = \frac{m_{Nf} + m_N}{m_S} \times 100 \quad (4)$$

Combining Equations (3) and (4) and re-arranging gives Equation (5).

$$\frac{\%N_s}{100} \times (m_f + \gamma m_N) = m_{Nf} + m_N \quad (5)$$

m_{Nf} is then replaced in Equation (5) using Equation (6):

$$m_{Nf} = \frac{\%N_f}{100} \times m_f \quad (6)$$

We define α, the ratio of adsorbed mass of N to the fresh sample mass, to re-arrange Equation (6) by dividing both sides by m_f.

$$\alpha = \frac{m_N}{m_f} \quad (7)$$

Combining Equations (5)–(7) allows α to be solved (Equation (8)).

$$\alpha = \frac{\%N_s - \%N_f}{100 - \gamma \%N_s} \quad (8)$$

Finally, converting the mass of adsorbed N to the mass of adsorbed NH_3 gives the adsorption capacity on a basis of mg of NH_3 adsorbed per g of fresh adsorbent mass ($\frac{m_{NH3}}{m_f}$, Equation (9)), which only makes use of the elemental analysis of the fresh and spent samples $\%N_f$ and $\%N_s$:

$$\text{Adsorption capacity}\left(\frac{mg_{\text{of NH3}}}{g_{\text{of fresh ads}}}\right) = 1000 \times \gamma\alpha = 1000 \times \gamma\left(\frac{\%N_s - \%N_f}{100 - \gamma \%N_s}\right) \quad (9)$$

Overall, each experiment condition yielded four adsorption capacities, generated due to the duplicate experiment and duplicate elemental analysis for each experiment.

2.2.7. Partial Pressure of Ammonia from Reaction Experiments of NaOH with $(NH_4)_2SO_4$ in Aqueous Solution

The following procedure is represented as 'Step 3' in Figure 1. In the closed system reaction between ammonium sulphate and sodium hydroxide in a water solution, a known amount of NH_3 gas product is generated in a finite headspace. Therefore, equilibria between the gaseous ammonia/aqueous ammonia and the moisture in the headspace/aqueous solution are expected to occur.

The total pressure in the headspace consequently depends on equilibrium amounts of gaseous NH_3 after reaction but also air and moisture. The liquid–vapour equilibrium of

NH_3 was determined by Henry's law (Equation (10)), while the liquid–vapour equilibrium of water was determined by Raoult's law (Equation (11)).

$$P_{NH3} = xH = yP_{tot} \quad (10)$$

$$x_{H2O,moist} \times P_{0,H2O,moist} = P_{H2O,moist} \quad (11)$$

In Equation (10), P_{NH3} is the equilibrium partial pressure of ammonia, x is the molar fraction of NH_3 in equilibrium in the aqueous liquid phase (dissolved ammonia), H is Henry's constant of ammonia (which is temperature dependent), y is the equilibrium NH_3 gas molar fraction after the reaction, and P_{tot} is the total pressure after the reaction. An essential assumption is that all of the NH_i product present in the liquid phase is only in its ammonia (NH_3) form (either gaseous or aqueous). This assumption is verified for solutions with pH > 11.

In Equation (11), $x_{H2O,moist}$ is the mole fraction of moisture in the gas phase before reaction, $P_{0,H2O,moist}$ is the vapour pressure of H_2O at the adsorption temperature (given by Antoine's equation), and $P_{H2O,moist}$ is the partial pressure of moisture in the gas phase, which is a contributing term to the total pressure in Equation (10).

2.2.8. Comparison of Adsorption Capacities to Isotherm Data from Literature

The majority of ammonia adsorption capacities found in the literature have been measured at a range of different conditions, including NH_3 partial pressures and adsorption temperatures.

In comparing the literature values to those derived from the present experiments, several approaches were taken to enable comparison at the same P_{NH3} and T_{ads} as those of the present study; these are represented as 'Step 4' in Figure 1. Whenever good fittings of experimentally measured adsorption capacities with adsorption equilibrium models were found in the literature, the models were first checked to reproduce the literature graphical representation of the adsorption isotherms. Subsequently, the quoted model equations and their parameters were used to interpolate the adsorption capacities to the conditions of the present study. Best fits for ammonia adsorption were obtained when using the adsorption equilibrium models of Dubinin–Astakhov, Toth, and Freundlich. In the absence of good model fits in the reference sources, graphical data extraction followed by cubic spline fitting was applied to obtain the interpolated data at the present study's partial pressures of ammonia and as close a temperature to 20 °C as possible.

The results section lists the approach used to generate the adsorption capacities at the three values of P_{NH3} of the present study and temperatures closest to 20 °C for a given literature reference and adsorbent. Generally, in the literature, the availability of graphical data of adsorption isotherms (adsorption capacity vs. pressures) exceeds that of model data. The partial pressures of ammonia covered in the literature can range from 10 mbar (1 kPa) to several bar (hundreds of kPa). In this study, pressures below 1.5 kPa were generated using the adsorption experiments. Therefore, whenever a graphical interpolation was used, the original figure data in the log scale of partial pressure were preferred to the linear scale, when available, due to the better graphical resolution in the low pressure range.

Dubinin–Astakhov Equilibrium Model

The Dubinin–Astakhov adsorption isotherm first requires the fitting of several datapoints and the identification of three isotherm parameters (see W_0, E and n in Equations (13)–(15)).

In the Dubinin–Astakhov model, it is assumed that the adsorbent houses the vapour adsorbate in a state similar to saturated liquid according to the Polanyi sorption potential theory [40].

The vapour pressure of the sorbate (P_0) can be calculated using Antoine's Equation (Equation (12)), where the equilibrium temperature (T_{eq}) is in Kelvin, and A, B, and C are component-specific Antoine constants. The constants and the format of Antoine's equation are obtained from the NIST chemistry webbook [41].

$$P_0 = 10^{\left(A - \frac{B}{T_{eq}+C}\right)} \quad (12)$$

At 20 °C, the vapour pressure of NH_3 is thus calculated to be 849.4 kPa. The adsorption capacity of a sample can be estimated, at a particular adsorption temperature (T_{ads}, in K) and ammonia partial pressure (P_{NH3}, in kPa), according to the Dubinin–Astakhov isotherm equations (Equations (13)–(15)) [42].

$$q = q_0 \times e^{\left\lfloor -\left(\frac{D}{E}\right)^n \right\rfloor} \quad (13)$$

$$D = RT_{ads}\ln\left(\frac{P_0}{P_i}\right) \quad (14)$$

$$q_0 = \rho W_0 \quad (15)$$

In Equations (13)–(15), 'q' is the adsorption capacity ($mass_{adsorbate}/mass_{adsorbent}$) where the 'adsorbate' here is NH_3 and the adsorbent is the solid sample tested. 'q_0' is the limiting adsorption capacity (same units as q), 'D' is the Polanyi adsorption potential (J/mol), 'E' is the characteristic energy of the adsorbent–adsorbate system (J/mol), and 'n' is the heterogeneity parameter (or pore dimensions, no units). 'R' is the universal gas constant (8.314 J $mol^{-1}K^{-1}$), and P_i is the partial pressure of the adsorbate (here P_i is P_{NH3}). T_{ads} is the adsorption temperature, and P_0 is the vapour pressure of the adsorbate (NH_3) at the defined adsorption temperature (=T_{eq} in Equation (12)). 'W_0' is the limiting pore volume of the adsorber bed material (cm^3 $mass_{ads}{}^{-1}$), and 'ρ' is approximated to be the liquid (or condensate) adsorbate density at the adsorption temperature.

The liquid density of the ammonia was determined with data by Haar and Gallagher [43], and a linear fit on temperature between −2 °C and 39 °C for saturated NH_3 was applied (Equation (16)), e.g., at 20 °C, $\rho_{NH3,liq}$ is 0.610 g cm^{-3}.

$$\rho_{NH_3,liq}\left(gcm^{-3}\right) = -1.439610 \times 10^{-3} \times T + 0.6388313 \quad (16)$$

Toth Equilibrium Model

The Toth model is a modification of the Langmuir model, which accounts for the presence of monolayer coverage. Whilst Langmuir assumes a homogenous surface, Toth assumes a heterogeneous surface with a variation of ammonia concentrations [44]. The adsorption capacity is calculated by Equation (17) [31]:

$$q_e = \frac{q_m bP}{\left[1 + (bP)^{t_0}\right]^{\frac{1}{t_0}}} \quad (17)$$

where q_e (mol kg^{-1}) is the adsorption at equilibrium, P (kPa) is the ammonia partial pressure at equilibrium, and q_m is the temperature-dependent maximum adsorbed capacity (Equation (18)).

$$q_m = q_{m0}e^{X\left(1 - \frac{T_{ads}}{T_0}\right)} \quad (18)$$

The temperature-dependent equilibrium constant, b (kPa^{-1}), in Equation (17), is calculated according to Equation (19).

$$b = b_0 e^{\left[\frac{Q}{RT_0}\left(\frac{T_0}{T_{ads}}-1\right)\right]} \quad (19)$$

The Toth heterogeneity factor, t_o (unitless), varies with temperature according to Equation (17).

$$t_o = t_{o0} + \alpha\left(1 - \frac{T_0}{T_{ads}}\right) \quad (20)$$

X and α are constants. The variables used at the reference temperature (T_0, K) are the maximum adsorbed capacity (q_{m0}, mol kg^{-1}), equilibrium constant (b_0, kPa^{-1}), and Toth heterogeneity factor (t_{o0}, unitless). R (J mol K^{-1}) is the ideal gas constant, and Q (J mol^{-1}) is the heat of adsorption.

Freundlich Equilibrium Model

The Freundlich isotherm at a given temperature is given by [45]:

$$q_c = K_F \times P^{\frac{1}{n}} \quad (21)$$

K_F ($cm^3g^{-1}kPa^{-1/n}$) and n (unitless) are constants, regarding the relative adsorption capacity of the adsorbent and the adsorption intensity.

Graphical Interpolation

In the cases where the literature did not present equilibrium adsorption model data but included adsorption isotherm data in graphical form, particularly those presented in log scale of partial pressure, the adsorption capacities were interpolated using the following procedure. Firstly, the scatter points from the isotherm curves were extracted using WebPlotDigitizer [46]. The extracted data points were then plotted as smoothed 1.5 point thickness curves in excel using only the pressure range 0–1.6 kPa. The smoothed curves were then uploaded once more in WebPlotDigitizer to extract full line data with 3–4 pixels in Δx and Δy resolutions. WebPlotDigitizer uses cubic spline interpolation to generate accurate data from graphical line curves.

2.2.9. Statistical Analysis

Univariate and multivariate statistical analyses were conducted using SPSS Statistics 28 to analyse the effects of treatment on the samples' ammonia adsorption performances and on the characteristics of the solids used for ammonia adsorption (molar ratios of hydrogen to carbon and oxygen to carbon, mass ratio of volatile matter to fixed carbon).

3. Results

Note all results shown in the results tables and figures can be found in the supplementary data file.

3.1. Characterisation of the Biosolids

3.1.1. Proximate and Ultimate Analyses

From the proximate and ultimate analysis of the untreated and treated biosolids (Tables 2 and 3), it can be seen that the untreated biosolids had a much higher volatile matter (VM) and lower fixed carbon (FC) content than their corresponding biochars. Generally, the treated biosolids had higher ash contents, which is known to happen as pyrolysis temperature increases [47]. The carbonisation of the treated biosolids is evident from the increase in the carbon contents (from 40–50 wt% to 70–80 wt%).

Table 2. Proximate analysis, ultimate analysis, and lignin contents of the untreated biosolids. Errors calculated by deviation from the mean. Samples analysed in duplicate. Given in wt% of as-received solid: moisture content (MC) and lignin. Given in wt% on dry basis of biosolid: volatile matter (VM), fixed carbon (FC), ash, C, H, N, S, and O. Definitions of sample abbreviations are provided in Section 2.1 (Materials).

Solids	DF Raw	GF Raw	NF Raw	NC Raw	ESF Raw	Oak Raw	CH	PeatSEPO	PeatMoss
MC	5.3 ± 0.1	4.8 ± 0.0	5.3 ± 0.0	3.8 ± 0.0	6.5 ± 0.6	-	4.5 ± 0.1	6.6 ± 0.1	6.5 ± 0.1
VM	72.9 ± 0.4	79.9 ± 0.0	70.3 ± 0.3	84.4 ± 0.0	78.9 ± 0.9	72.5 ± 6.0	63.7 ± 2.7	64.0 ± 0.3	61.3 ± 1.9
FC	26.8 ±0.5	20.0 ± 0.0	29.5 ± 0.3	13.4 ± 0.0	20.5 ± 1.5	24.7 ± 4.8	28.2 ± 0.5	31.1 ± 0.0	28.2 ± 0.3
Ash	0.4 ± 0.1	0.1 ± 0.0	0.2 ± 0.1	2.2 ± 0.0	0.6 ± 0.6	4.2 ± 1.3	8.0 ± 3.2	4.8 ± 0.3	10.6 ± 1.7
C	49.7 ± 1.0	47.8 ± 0.0	54.1 ± 0.5	50.0 ± 1.8	44.7 ± 4.5	43.4 ± 2.1	48.4 ± 1.5	48.6 ± 0.2	43.3 ± 1.7
H	5.1 ± 0.5	5.9 ± 0.1	5.7 ± 1.1	6.0 ± 0.3	5.0 ± 0.5	5.9 ± 0.1	3.8 ± 0.1	3.9 ± 0.4	3.0 ± 0.3
N	0.6 ± 0.0	0.7 ± 0.0	0.7 ± 0.0	0.7 ± 0.0	1.0 ± 0.0	0.3 ± 0.2	0.8 ± 0.1	2.5 ± 0.0	2.1 ± 0.2
S	0.0 ± 0.0	0.0 ± 0.0	0.0 ± 0.0	0.0 ± 0.0	0.0 ± 0.0	0.1 ± 0.0	0.0 ± 0.0	0.3 ± 0.0	0.1 ± 0.1
O	44.3 ± 0.1	45.6 ± 0.0	39.4 ± 1.6	43.3 ± 0.1	48.7 ± 0.5	42.9 ± 1.0	38.9 ± 1.8	39.8 ± 0.6	41.0 ± 1.9
Lignin	32.3 ± 0.5	22.2 ± 0.2	48.3 ± 1.0	14.8 ± 0.6	45.0 ± 1.0	25.0 ± 1.1	57.3 ± 11.9	57.9 ± 1.8	42.6 ± 0.1

Table 3. Proximate and ultimate analysis of the treated biosolids. Samples analysed in duplicates. Error calculated by deviation from the mean. Same nomenclature as Table 2 is used. 'bc' stands for 'biochar'. Definitions of sample abbreviations are provided in Section 2.1 (Materials).

Solids	DF bc	DF HWbc	NF bc	NF HW bc	NC bc	ESF bc	Oak bc	NORIT-AC	SIGMA-AC
MC	2.2 ± 0.3	1.9 ± 0.1	2.4 ± 0.2	3.5 ± 0.5	4.6 ± 0.5	2.1 ± 0.2	2.8 ± 0.7	1.6 ± 0.3	3.0 ± 0.4
VM	27.4 ± 5.1	22.1 ± 0.2	23.2 ± 0.3	29.7 ± 0.4	25.1 ± 0.5	22.3 ± 0.9	23.9 ± 4.6	3.7 ± 0.3	17.5 ± 1.0
FC	68.7 ± 4.1	73.1 ± 0.6	74.8 ± 0.9	69.8 ± 0.5	65.8 ± 0.5	72.9 ± 1.2	69.8 ± 7.0	92.2 ± 3.5	74.3 ± 0.0
Ash	3.9 ± 1.0	4.8 ± 0.5	2.0 ± 1.2	1.4 ± 1.1	9.1 ± 0.0	4.8 ± 0.3	6.3 ± 2.3	8.2 ± 1.0	8.3 ± 1.0
C	75.9 ± 0.0	73.6 ± 0.9	74.3 ± 1.5	75.9 ± 0.3	70.9 ± 0.8	73.1 ± 1.8	74.3 ± 2.6	85.8 ± 0.9	68.4 ± 0.7
H	2.6 ± 0.0	2.6 ± 0.2	2.5 ± 0.1	2.4 ± 0.0	2.6 ± 0.0	2.6 ± 0.1	1.8 ± 0.3	0.1 ± 0.0	0.9 ± 0.1
N	2.7 ± 0.1	0.7 ± 0.1	2.4 ± 0.1	0.6 ± 0.0	2.6 ± 0.2	2.7 ± 0.1	1.3 ± 0.0	1.3 ± 0.0	1.1 ± 0.0
S	0.0 ± 0.0	0.0 ± 0.0	0.0 ± 0.0	0.0 ± 0.0	0.0 ± 0.0	0.0 ± 0.0	0.0 ± 0.0	0.5 ± 0.0	0.0 ± 0.0
O	14.9 ± 0.0	18.4 ± 1.0	18.8 ± 1.5	19.7 ± 0.3	13.8 ± 1.0	16.7 ± 2.0	16.3 ± 2.4	4.1 ± 0.9	21.3 ± 0.6

The reduction in O and H after treatment is due to the heating from the pyrolysis providing sufficient energy to break functionalities around the samples' structures [48], which contain mostly oxygen and hydrogen.

From the lignin determination of the untreated ('Raw') biosolids (Table 2), it can be seen that most of them had high levels of lignin, with a mean of 36.7 ± 1.0 wt% over the nine biosolids tested.

3.1.2. Metals Content in the Untreated Biosolids

As in some studies, metal doping of activated carbons was used to increase their adsorption capacity. In this study, the metal content in the biosolids was determined to investigate a possible correlation between the concentration in metals naturally present in the biosolids and their adsorption capacity. Atomic absorption spectroscopy measurements of the main metals in the untreated biosolids are listed in Table 4 in order of decreasing value. Calcium and potassium were the two main metals present, at a combined average content five times that of the combined average content of the other four metals (magnesium, sodium, aluminium, and iron) with 7.1 mg/g vs. 1.4 mg/g, respectively. The large presence of Ca and K in the tree residue samples was expected, as they are essential for tree growth [49].

Table 4. Atomic absorption spectroscopy (AAS) of untreated biosolids. All values in mg/g. Error values were calculated by deviation from the mean.

Untreated Biosolid	Ca	K	Mg	Na	Al	Fe
DF Raw	3.9 ± 0.7	1.6 ± 0.1	0.8 ± 0.0	0.6 ± 0.1	0.6 ± 0.1	0.3 ± 0.0
GF Raw	2.2 ± 0.2	2.7 ± 0.1	0.6 ± 0.0	0.0 ± 0.0	0.2 ± 0.0	0.0 ± 0.0
NF Raw	2.7 ± 0.2	1.2 ± 0.1	0.7 ± 0.0	0.2 ± 0.1	0.0 ± 0.0	0.0 ± 0.0
NC Raw	10.0 ± 0.5	2.8 ± 0.1	0.9 ± 0.2	0.3 ± 0.0	0.3 ± 0.1	0.0 ± 0.0
ESF Raw	5.0 ± 0.2	2.1 ± 0.0	0.7 ± 0.0	0.4 ± 0.1	0.0 ± 0.0	0.1 ± 0.0
CH	0.7 ± 0.0	7.8 ± 1.0	0.7 ± 0.1	1.1 ± 0.1	0.0 ± 0.0	0.1 ± 0.0
Means	4.1 ± 0.3	3.0 ± 0.2	0.7 ± 0.1	0.4 ± 0.1	0.2 ± 0.0	0.1 ± 0.0

3.2. Calculation of Partial Pressure of NH_3 from Reaction Experiments of NaOH with $(NH_4)_2SO_4$

Some of the main outputs related to the calculation of P_{NH3} (Step 3, Figure 1) are provided in Table 5 for the three experiments detailed in Table 1. Figure 2 plots x (liquid mol fraction of NH_3) and y (gaseous mol fraction of NH_3) as functions of total ammonia moles for each experiment.

Table 5. Experimental conditions pre- and post-NaOH/$(NH_4)_2SO_4$ reaction, leading to calculated partial pressures of NH_3 assuming equilibrium conditions by end of adsorption experiment. Temperature 20 °C; starting total pressure 100 kPa.

Experiment at 20 °C	0.05 mol L^{-1}	0.5 mol L^{-1}	1.8 mol L^{-1}
Pre-NaOH/$(NH_4)_2SO_4$ reaction			
$(NH_4)_2SO_4$: (g) – (moles)	0.17 – 0.0013	1.68 – 0.0127	5.91 – 0.0447
NaOH: (g) – (moles)	0.25 – 0.0063	2.47 – 0.0618	7.42 - 0.1855
Gas volume (cm^3)	165.2	167.1	171.6
H_2O vapour (moles)	1.58×10^{-4}	1.57×10^{-4}	1.56×10^{-4}
Post-NaOH/$(NH_4)_2SO_4$ reaction			
Concentration NaOH (mol L^{-1})	4.34×10^{-2}	4.38×10^{-1}	1.23
pH (based on excess NaOH)	12.6	13.6	13.9
$NH_{3\ tot}$ (moles), assuming no NH_4^+	2.57×10^{-3}	2.542×10^{-2}	8.943×10^{-2}
x ($NH_{3\ (l)}$ mol fraction)	5.5×10^{-4}	5.44×10^{-3}	1.955×10^{-2}
y ($NH_{3\ (g)}$ mol fraction)	3.9×10^{-4}	3.91×10^{-3}	1.391×10^{-2}
$NH_{3\ (g)}$ moles= total minus liq.	2.735×10^{-6}	2.7557×10^{-5}	1.01597×10^{-4}
Total liquid moles	4.70231	4.66360	4.56988
Volume Liquid (mL)	84.79	82.88	78.37
Total gas moles (air + $NH_{3(g)}$ + moisture)	6.9427×10^{-3}	7.0453×10^{-3}	7.3029×10^{-3}
P_{tot} Total Pressure post-reaction (kPa)	102.37	102.69	103.65
Henry's cst. $_{aq}NH_3$ @ 20 °C (kPa)		73.77	
% rel. err. Equation (10) (Solver)	0.022	0.001	0.008
Excel Solver Solution P_{NH3} (kPa)	0.040	0.402	1.442

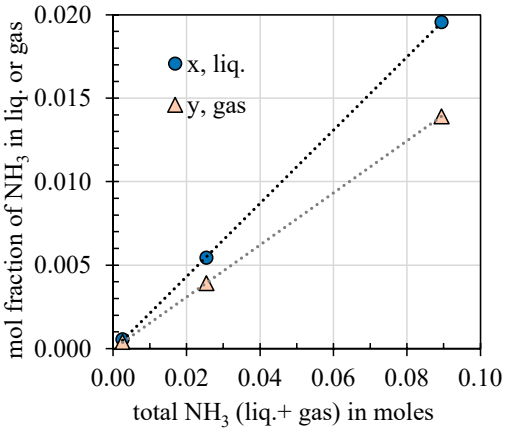

Figure 2. Molar fractions of NH_3 in the equilibrium aqueous solution (x) and in the gas (y) vs. the total moles of NH_3 for the three experiments.

Table 5 confirms that as expected from the experimental methodology, the total moles of NH_3 (gas + liq) increase with the increased concentration of $(NH_4)_2SO_4$ used initially, but the total equilibrium moles in the liquid decrease. This is due to the increased yield of gaseous NH_3, as intended. Figure 2 illustrates that both molar fractions x and y increase linearly with the total NH_3 moles present in the bottles. However, for increasing concentration of $(NH_4)_2SO_4$, the fraction of dissolved NH_3 (aqueous NH_3) increased more comparatively to the gaseous NH_3 fraction, as an effect of the increase in total pressure following Henry's law and also of the lower amount of liquid moles. The methodologies described in 2.2.6 and 2.2.7 which supplement 2.2.5 were designed for the purpose of constructing adsorption isotherms comparable to those found in the literature.

3.3. Review of NH_3 Adsorption Capacities of Common Adsorbents, Interpolated to 0–20 °C and Below 1.5 kPa

As part of Step 4, with the aim of providing validation data to the experimental methodology set up to derive NH_3 adsorption capacities from tabletop batch reaction experiments of NaOH with $(NH_4)_2SO_4$ in aqueous solution, two commercial activated carbons were tested, and their capacities were compared to those found in the literature for similar materials in the same conditions. This exercise also provided an opportunity to review all types of NH_3 adsorbents. This section and the next show these results.

The adsorbents listed in Table 6 cover a wide range of materials, including the organic (activated carbons first, as closest to our biosolids) and mineral sources used previously for ammonia adsorption. In order from lowest to highest capacity, we find first, activated carbons, followed by alumina, silica, and zeolites, in the same order for the three values of P_{NH3}. Among the mineral adsorbents, the zeolites' mean capacity of 63.3 mg/g (n = 6) at 1.44 kPa and temperatures 0–20 °C exhibited the largest standard deviation (SD) of 43.8 mg/g. Comparatively, both alumina, with a mean of 21.4 mg/g (n = 3) and SD 1.9 mg/g, and silica adsorbents, with a mean of 42.3 mg/g (n = 7) and SD 9.5 mg/g at 1.44 kPa and 20–30 °C, exhibited much lower variation. The carbon adsorbents are discussed separately below due to their organic nature and also as a basis for validation of the experimental methodology.

Table 6. Ammonia adsorptions of common organic and mineral adsorbents collated from literature. Key to methods of comparison: 'D-A' Dubinin–Astakhov, 'Fr'. Freundlich, 'CuSpl' cubic spline interpolation, 'LinInt' linear interpolation between two temperatures' data.

Name of Sample	Partial Pressure of NH_3 (kPa)			R^2	Method of Comparison	Ref.
	0.04	0.40	1.44			
Activated Carbon						
Merck @ 293K	0.5	1.9	4.4	0.99	D-A	[50]
SP Défense Undoped @ 293K	0.1	0.7	2.6	0.99	Toth	[31]
SP Défense $ZnSO_4$-Doped AC @ 293K	9.5	25.0	40.2	0.96	Toth	[31]
Chemviron—Coconut Shell ('CS') LM127 @ 293K	22.0	40.6	57.3	n.a.	D-A	[51]
AC-OS-CO_2 1 @ 293K	0.7	3.3	8.1	1.00	Fr	[45]
AC-OS-H_2O 2 @ 293K	0.1	0.9	2.8	1.00	Fr	[45]
AC-OS-KOH 2-900 @ 293K	2.0	8.4	18.6	1.00	Fr	[45]
AC-OS-H_3PO_4 1 @ 293K	5.0	13.6	23.5	1.00	Fr	[45]
Norit C Gran @ 293K	4.5	12.5	22.0	1.00	Fr	[45]
Norit GAC 1240 @ 293K	0.2	1.1	3.0	1.00	Fr	[45]
AC-M1 @ 298K	0.8	3.1	5.8	n.a.	CuSpl	[52]
AC-M2 @ 298K	10.3	19.7	29.5	n.a.	CuSpl	[52]
AC-M3 @ 298K	2.8	24.7	43.7	n.a.	CuSpl	[52]
AC-M4 @ 298K	4.8	21.6	29.7	n.a.	CuSpl	[52]
Mean of Activated Carbons 21.2 mg/g, SD 16.1 mg/g @1.44 kPa						

Table 6. *Cont.*

Name of Sample	Partial Pressure of NH_3 (kPa)			R^2	Method of Comparison	Ref.
	0.04	0.40	1.44			
Alumina						
Alumina @ 293K	11.7	17.8	22.7	0.99	D-A	[50]
Alumina @ 293K	8.2	14.1	18.7	n.a.	Toth + LinInt.	[53]
Alumina @ 293K	11.7	17.9	22.7	n.a.	Int.	[51]
Mean of Alumina 21.4 mg/g, SD 1.9 mg/g @ 1.44 kPa						
Silica (key: OMS = ordered mesoporous silica)						
Silica Gel @ 293K	15.5	29.3	39.8	0.99	D-A	[50]
Silica Gel @ 293K	10.2	19.1	27.1	n.a.	D-A	[51]
OMS Superacids @ 298K	0.8	6.9	22.1	n.a.	CuSpl	[54]
OMS-SO_3H-0.1 @ 298K	1.5	20.9	42.9	n.a.	CuSpl	[54]
OMS-SO_3H-0.2 @ 298K	2.4	28.6	55.7	n.a.	CuSpl	[54]
OMS-SO_3H-0.5 @ 298K	1.5	20.9	43.8	n.a.	CuSpl	[54]
OMS-SO_3H-1.0 @ 298K	1.6	19.3	48.0	n.a.	CubSpl	[54]
Mean of Silica 42.3 mg/g, SD 9.5 mg/g @1.44 kPa						
Zeolite						
4A @ 293K	58.5	92.8	111.4	0.99	D-A	[50]
13X @ 293K	61.7	94.5	112.9	0.99	D-A	[50]
13X @ 293K	42.3	62.9	78.5	n.a.	D-A	[51]
NaP w/$Al(O\text{-}ipr)_3$ @ 273K	13.4	18.1	21.8	n.a.	CuSpl	[55]
NaP w/$Al(OH)_3$ @ 273K	26.2	33.8	40.3	n.a.	CuSpl	[55]
NaP w/$NaAlO_2$ and sodium silicate @ 273K	4.2	13.0	14.9	n.a.	CuSpl	[55]
Mean of Zeolite 63.3 mg/g, SD 43.8 mg/g @1.44 kPa						

3.4. Validation of Experimental Methodology on Activated Carbons

Within the activated carbons, a mean capacity of 21.2 mg/g was found at 1.44 kPa and 20 °C for 14 materials from the literature, albeit with a very large standard deviation (16.1 mg/g), illustrated by the lowest value 2.6 mg/g (SP Défense, undoped [31] and highest at 57.4 mg/g (Chemviron's coconut shell monolithic LM127 [51]). The latter appeared as an outlier, but no information could be found on its manufacturing process to explain its high adsorption. In order to test this work's experimental methodology, the adsorption capacities of two commercially sourced activated carbons were investigated in the batch reaction experiments.

Figure 3 plots the NH_3 adsorption capacities at 20 °C and 1.44 kPa of the two AC materials measured in this work (Norit RO 3515, and Sigma Aldrich), as well as those interpolated for the other AC from the literature and listed in Table 6, in order of increasing capacity.

Despite activated carbons being known for their adsorbency properties [45,56–61], the two commercially sourced materials tested had very low capacities at P_{NH3} of 1.44 kPa, with less than 6 mg/g. These values were close to many of the capacities interpolated from the literature at 20 °C and 1.44 kPa for undoped and untreated activated carbons, notably, this work's Norit AC RO 3515 (2.7 mg/g) with [31]'s SP Défense undoped's 2.6 mg/g, as well as [45]'s Norit GAC 1240's 3.2 mg/g. Furthermore, this work's Sigma Aldrich's 5.9 mg/g was close with Merck's 4.4 mg/g [50]. Overall, the larger values were obtained for strong base-treated (KOH), weak acid-treated (H_3PO_4), or doped ($ZnSO_4$) activated carbons. A few other activated carbons of unknown origin also exhibited high capacities (AC-M2-4 [52]).

The NH_3 adsorption capacities of the hot-water-washed biochars in this study (16.3–16.7 mg/g at 1.44 kPa_{NH3}) were higher than all of the undoped and unmodified ACs in the literature but lower than all doped and modified ACs. The benefit of modifying ACs for increasing ammonia adsorption capacity is illustrated by Cardenas et al. [31], where the doped AC was impregnated with zinc sulphate to improve the hydrophilic

characteristics. There appears to be a positive effect of higher metal ion (Cu^{2+}, Fe^{3+}, Zn^{2+}, Ni^{2+}) concentration on hydrophilicity [62].

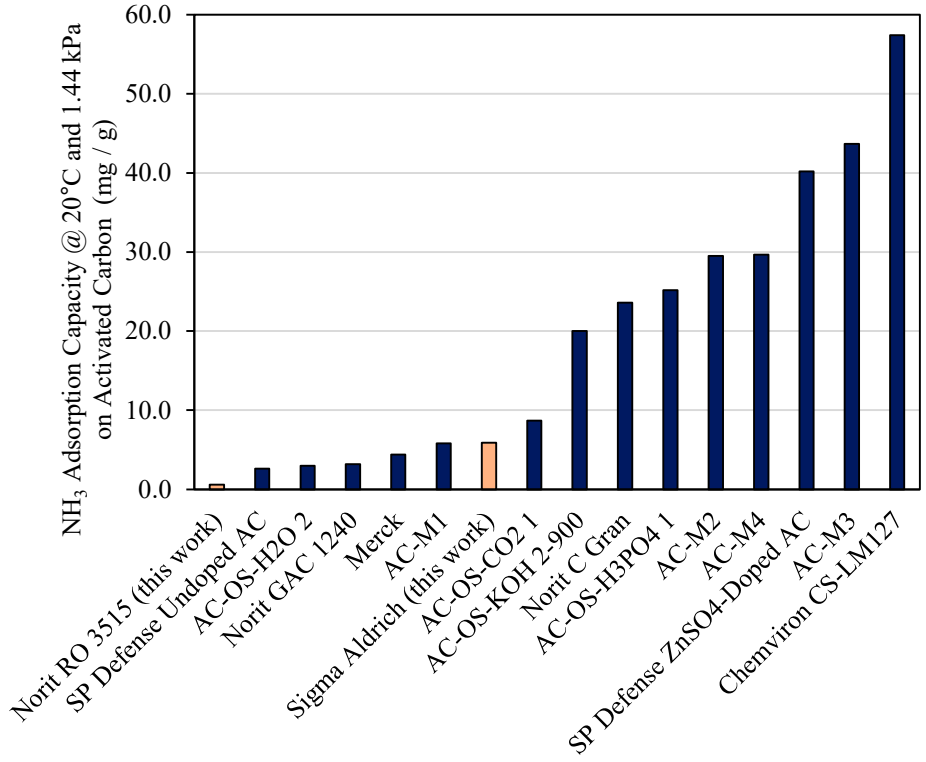

Figure 3. NH_3 Adsorption capacities at 293 K and 1.44 kPa of two commercially sourced activated carbon materials ('AC') measured in this work (in orange) compared to those of 14 other AC interpolated data from the literature, in dark blue (Table 6). AC-OS = activated carbon from pyrolysis of olive stones (31). CS = activated carbon from coconut shell (Chemviron manufacturer).

Corroboration of the capacities obtained in this work on commercially sourced undoped activated carbons by three different literature sources [31,45,50] provided a good measure of validation for the methodology of the tabletop batch reaction experiments of NaOH with $(NH_4)_2SO_4$ in aqueous solution reported here. The differences between the adsorption capacities of activated carbon samples in this study compared to those found in the literature may be due to a number of factors, including the experimental method of adsorption, the particle size of the material, and the source and composition of the samples.

3.5. Adsorption Capacities of Untreated Lignin-Rich Biosolids

The breadth of samples run in this study were first separated into 'Untreated' and 'Treated' categories, where the five raw tree barks, one wood (oak), coconut husk, and the two peats belonged to the 'Untreated' category, and the biochars produced by the slow pyrolysis of the untreated biosolids, the two commercial activated carbons, and the two washed biochars were considered 'treated' by either washing, pyrolysis, and/or activation (Table 7). Each sample that underwent the reaction experiments of NaOH with $(NH_4)_2SO_4$ (in duplicate) had their nitrogen content measured in duplicate by elemental analysis; this resulted in four adsorption capacities being derived for each sample.

The 'Untreated' biosolids tested in the present study exhibited much higher adsorption capacities than common, undoped, non-acid- or base-treated commercially sourced activated carbons. Across the untreated barks tested, the Douglas-fir bark performed best, with 41.6 mg/g at 1.44 kPaNH_3. The DF had similar results to the untreated oak, which had an adsorption capacity of 41.9 mg/g at 1.44 kPaNH_3. Untreated barks from

the grand fir and noble fir performed similarly to each other at 1.44 kPa (27.7–28.8 mg/g). At 0.04 kPa, untreated barks from the noble fir and European silver fir had the highest ammonia adsorption (20.2–23.4 mg/g). The two untreated peats and the coconut husk consistently delivered comparatively high adsorption capacities (>27 mg/g at 1.44 kPa).

Table 7. Ammonia sorption capacity (values in mg of NH_3/g fresh adsorbent) of all samples in this study. Reported errors calculated over 4 measurements.

Untreated Biosolids	**0.04 kPa**	**0.40 kPa**	**1.44 kPa**
Douglas-fir—Raw	14.9 ± 1.6	34.9 ± 1.8	41.6 ± 1.0
Grand fir—Raw	13.3 ± 0.9	22.9 ± 2.2	28.8 ± 2.0
Noble fir—Raw	23.4 ± 3.7	26.5 ± 3.0	27.7 ± 1.2
Nootka cypress—Raw	11.9 ± 4.9	14.4 ± 0.8	17.6 ± 0.1
European silver fir—Raw	20.2 ± 1.3	20.2 ± 1.7	19.6 ± 1.2
Oak—Raw	19.6 ± 2.5	28.0 ± 1.4	41.9 ± 0.5
Coconut husk	11.6 ± 5.2	24.1 ± 2.5	27.3 ± 2.8
Irish peat	4.4 ± 3.3	17.2 ± 0.9	29.2 ± 7.2
Moss sphagnum peat	5.6 ± 1.9	20.8 ± 2.1	27.4 ± 3.8
Treated Biosolids	**0.04 kPa**	**0.40 kPa**	**1.44 kPa**
Douglas-fir—Biochar	−15.6 ± 0.6	−12.8 ± 0.4	−11.5 ± 0.4
Douglas-fir—Hot-water-washed biochar	3.9 ± 1.3	17.5 ± 2.7	16.7 ± 1.0
Noble fir—Biochar	−9.2 ± 1.8	−7.2 ± 2.2	−5.3 ± 1.3
Noble fir—Hot-water-washed biochar	6.1 ± 0.6	18.1 ± 0.7	16.3 ± 0.9
Nootka cypress—Biochar	−16.2 ± 14.2	−12.3 ± 11.1	−9.9 ± 0.2
European silver fir—Biochar	−12.9 ± 2.0	−8.1 ± 0.3	−7.1 ± 0.6
Oak—Biochar	−2.4 ± 5.0	10.6 ± 1.9	11.6 ± 7.0
NORIT-Activated Carbon	0.0 ± 0.6	2.7 ± 0.9	0.6 ± 1.2
SIGMA-Activated Carbon	−8.2 ± 1.0	4.3 ± 0.3	5.9 ± 1.2

The greatest capacity reached in this study (41.9 mg/g in untreated Oak) is similar to the AC-M1 [52] and SP Défense ZnSO4-doped AC [31], one of the rare examples to date of metal-doped AC for ammonia adsorption. The high ammonia adsorption capacity of the untreated oak may be due to its high levels of chemical functionality. This can be seen from the high oxygen contents from the elemental analysis and reasonable levels of lignin inferring the oak's complex structure. Most of the untreated biosolids in this study had greater adsorption capacities than most of the ACs in the literature, except for AC-M2, AC-M4 [52], and Chemviron's LM127 [51].

The only zeolites that had capacities similar to those obtained for the biosolids in this study were the ones tested by Lucero et al. [55]. The remaining zeolites had higher adsorption capacities relative to those measured in this study. Zeolites are known for being high-performance adsorbents with well-defined pore sizes and the ability to be fine-tuned to improve adsorption properties due to their structural and compositional richness [63].

It has been posited by Wojtowicz et al. [64] that the ideal pore size for ammonia adsorption is between 0.9–2.2 nm. These dimensions are small enough to allow strong van der Waals forces whilst being sufficiently large for ammonia molecules to enter the microporous structure of the sorbent. Nevertheless, zeolites are expensive materials with poor sustainability [65] due to their energy intensive chemical synthesis [66].

The range of the adsorption capacities found in the literature for alumina and silica are somewhat similar to those of the untreated biosolids. However, alumina and silica may be also expected to be less sustainable than the untreated biosolids examined in the study due to mining in their production process [67–70]. Overall, low-cost materials such as untreated barks, with expected high levels of sustainability, merit being compared alongside conventional commercial materials when selecting potential NH_3 adsorbents due to similar performance in adsorption at low partial pressures of ammonia.

All of the biochars produced by slow pyrolysis in our experiments (except for oak) exhibited negative NH_3 adsorption capacities, caused by measuring a higher value of

$\%N_f$ (wt% of N in the fresh sample) compared to $\%N_S$ (wt% N in the spent sample) in Equation (6). This was likely due to the pyrolysis process depositing nitrogen onto the biochars, and as the oak biochar was supplied externally, the oak sample did not have the same issue. Takaya et al. [32] also found that untreated oak had greater sorption potential than their biochars produced above 450 °C.

In order to address the issue of nitrogen upload after the pyrolysis and before the NH_3 adsorption experiments, the biochars from Douglas-fir and noble fir were washed in hot water after pyrolysis (Table 8), and the elemental analysis was repeated after hot water washing. The nitrogen contents were seen to decrease after water washing and pre-NH_3 adsorption, allowing more nitrogen to be adsorbed later on in the reaction experiments. The hot-water-washed biochars ended up outperforming some of the common activated carbons (Table 7), with medium capacities 16–17 mg/g at 1.44 kPa, although they were still lower than those of the untreated biosolids.

Table 8. Change in base nitrogen contents of biochars before and after hot water washing.

Sample	Form of Sample	Nitrogen Content From CHNS (wt%)
DF	Biochar	2.68 ± 0.05
	Hot-water-washed biochar	0.67 ± 0.05
NF	Biochar	2.39 ± 0.08
	Hot-water-washed biochar	0.57 ± 0.01

3.6. Statistical Results

Figure 4a,b provide bar plots of the adsorption capacities of the untreated (Figure 4a) and treated (Figure 4b) biosolids on the same scale of adsorption capacity for the experiments at partial pressure of NH_3 of 1.44 kPa and 20 °C, for which the highest adsorptions were obtained.

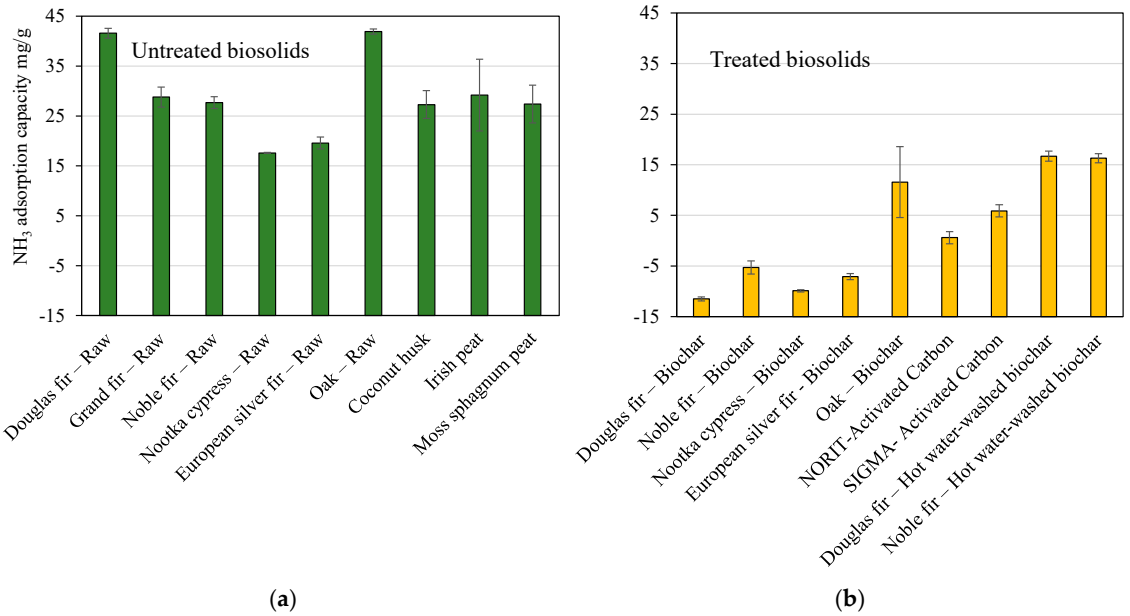

(**a**) (**b**)

Figure 4. NH_3 adsorption capacities of this work's biosolids at P_{NH3} of 1.44 kPa in mg of NH_3 per g of fresh adsorbent. (**a**) Untreated biosolids (barks, peats, coconut husk); (**b**) Treated biosolids (unwashed and water-washed biochars of materials listed in (**a**). Same ordinate scale is used for (**a**) and (**b**) for direct comparison. Error bars are deviation from the mean over 4 measurements.

The clear difference in ranges of adsorption between lack of treatment and treatment for a given biosolid, as well as overall across all biosolids, indicates a statistical analysis of the factor 'treatment' on NH_3 adsorption capacity using the two levels of treatment

(untreated and treated) could reveal effects with statistical significance. This correlation between the sample treatment and the adsorption capacity was explored using univariate analysis. All unaveraged data were input into the software (SPSS Statistics 28), where the samples were separated into the levels (or categories) 'untreated' and 'treated' (Table 9), covering a total of 224 measurements of adsorption capacity at all the pressures tested, 112 of which were tested on untreated biosolids. Furthermore, in Table 9, which presents the pairwise comparisons between the two levels of factor 'treatment', it can be seen that the effect of treatment level on the ammonia adsorption capacity is significant ($p < 0.001$).

Table 9. Univariate statistical analysis descriptive statistics and pairwise comparison outputs of ammonia adsorption capacity (mg/g) against sample treatment.

Descriptive Statistics			
Treatment	Mean	Std. Deviation	N
Untreated	22.03	9.40	112
Treated	−1.26	10.92	112
Total	10.38	15.47	224
Pairwise Comparisons			
Treatment	Treatment	Std. Error	*p*
Untreated	Treated	1.36	<0.001

The mean values of ammonia adsorption capacities of untreated and treated samples for each P_{NH3} were plotted with their respective error bars using standard deviations generated by the statistical analysis (Figure 5).

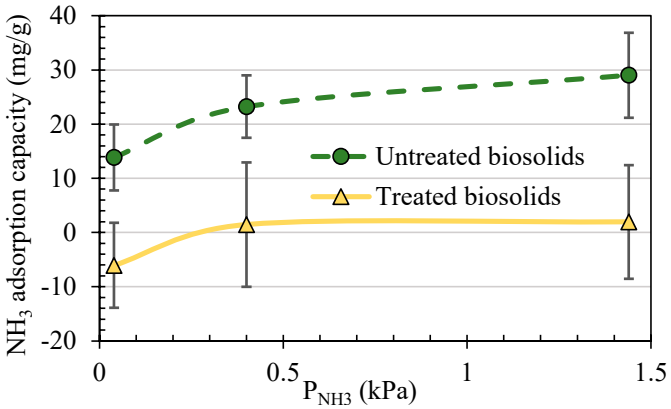

Figure 5. Comparison of the averages of ammonia adsorption capacities of the untreated biosolids (raw barks, oak, and peats) and treated biosolids (biochars and activated carbons). Error bars are 1× standard deviation (N = 112).

In Figure 5, the error bars for each of the three partial pressures do not overlap at any point, which further illustrates that the differences between the two levels of treatment were statistically significant.

As there was a clear difference between the untreated and treated biosolids in terms of adsorption capacity, possible reasons for the difference between the two levels of treatment were explored by comparing the molar H/C and O/C ratios and the mass ratio of volatile matter to fixed carbon using multivariate statistical analysis (Tables 10 and 11). From the statistical analysis, the effect of the biosolid treatment level on all three ratios was significant ($p < 0.01$). The means and standard deviations from Tables 10 and 11 were used to produce Figure 6.

Table 10. Multivariate statistical analysis descriptive statistics output of volatile matter/fixed carbon mass ratio, molar H/C, and O/C ratios of untreated and treated biosolids.

	Treatment	Mean	Std. Deviation	N
Mass ratio VM/FC db	Untreated	3.33	1.43	18
	Treated	0.40	0.31	18
	Total	1.87	1.81	36
Molar H/C	Untreated	1.20	0.21	18
	Treated	0.33	0.13	18
	Total	0.76	0.47	36
Molar O/C	Untreated	0.67	0.11	18
	Treated	0.16	0.06	18
	Total	0.42	0.27	36

Table 11. Multivariate statistical analysis pairwise comparison output of volatile matter/fixed carbon mass ratio, molar H/C, and O/C ratios of untreated and treated biosolids.

	Treatment	Treatment	Std. Error	*p*
VM/FC db	Untreated	Treated	0.346	<0.01
Molar H/C	Untreated	Treated	0.059	<0.01
Molar O/C	Untreated	Treated	0.029	<0.01

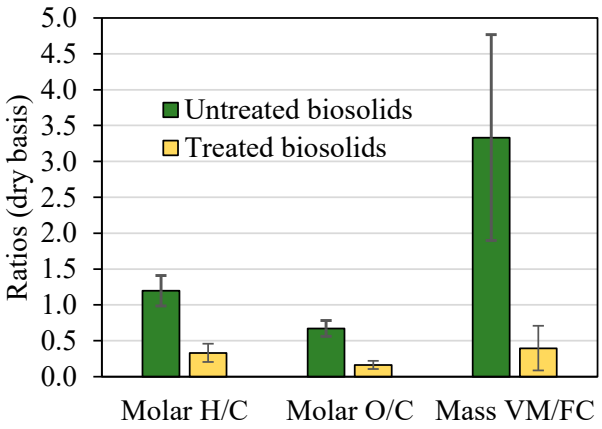

Figure 6. Means of molar H/C, molar O/C, and volatile matter/fixed carbon ratio values for the untreated and treated biosolids. Error bars are 1× standard deviation (N = 18).

Here, the largest difference was in the volatile matter/fixed carbon (VM/FC) ratio after slow pyrolysis. In the pyrolysis process, volatile components are expected to leave the structure of the biomass, while the fixed carbon remains [71]. This is why the VM/FC is expected to be lower for the treated biosolids rather than untreated biosolids.

In addition to surface area, a factor that is known to impact adsorption capacity is the amount of functional groups in the adsorbent [72]. The functional groups that are present on the surface of the biomass reduce through the pyrolysis process [32]. These groups are volatile organic compounds, such as phenols, alcohols, and aromatics [73]. It can therefore be theorised that as the volatile matter of the sample decreases, the extent of functional groups decreases also, reducing the VM/FC ratio and thus the NH_3 adsorption capacity.

The molar H/C and O/C decreases after slow pyrolysis. The reduction in O and H is likely due to the heating from the pyrolysis providing sufficient energy to break functionalities around the samples' structures [48], which contain mostly oxygen and hydrogen. The loss of O and H thereby carbonises the sample, increasing its proportion of carbon.

For a more detailed look into the effect of biosolid treatment, the values of the VM/FC, molar H/C, and O/C ratio were directly compared for each biosolid type (Figure 7).

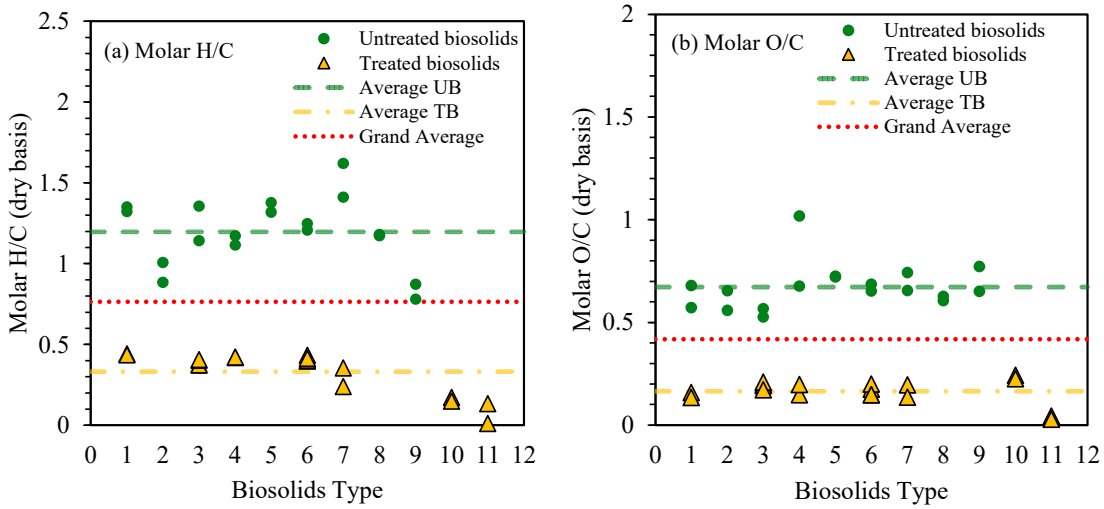

Figure 7. Comparison of (**a**) molar H/C and (**b**) molar O/C ratios for untreated and treated biosolids. Each number on the x axis represents one type of biosolid for which untreated and treated elemental analysis was carried out. Experiments were carried out in duplicate in some cases for both levels of treatment, e.g., there are 2 points for both untreated and treated types 3 and 7. Key to biosolid type: 1-NC, 2-CH, 3-NF, 4-ESF, 5-GF, 6-DF, 7-Oak, 8-PeatSEPO, 9-PeatMoss, 10-SIGMA AC, 11-NORIT-AC.

From Figure 7, the change in molar H/C and O/C can be assumed to be due to the change in lignocellulosic composition, with the molar ratios providing an indication as to how they were affected by the pyrolysis process. The untreated biosolids have higher molar H/C and molar O/C values than their associated treated samples. This is expected due to the increasing carbon contents gained by the carbonisation that occurs from pyrolysis. During pyrolysis (at 400 and 450 °C in this study), cellulose and hemicellulose degrade at 300 °C and between 300–340 °C respectively [74]. From the assumed molar H/C and O/C ratios for the lignocellulosic components (in Table 12), it can be observed that the H/C and O/C of cellulose and hemicellulose have at least double the value than that of lignin's. Therefore, as the proportion of lignin grows after pyrolysis (from cellulose and hemicellulose degradation), the molar H/C and O/C values would reduce.

Table 12. Estimated molar H/C and molar O/C ratio of lignocellulosic components [75–77].

Component	Assumed Empirical Formula	Molar H/C	Molar O/C
Lignin	$C_9H_{10.2}O_{3.4}$	0.09	0.50
Cellulose (Glucose)	$C_6H_{12}O_6$	0.17	1.33
Hemicellulose (Xylose)	$C_5H_{10}O_5$	0.17	1.33

Finally, when comparing the metals content between untreated and treated biosolids, from the atomic absorption spectroscopy of the untreated biosolids (Table 4), low concentrations of Fe were measured, and no significant effect of Fe^{3+} ions was found on ammonia adsorption capacity. The untreated biosolids in this study had higher concentrations of calcium and potassium, but there does not seem to be any recorded correlation between their concentrations and the adsorption capacity, and this study did not find any.

4. Conclusions

A low cost, safe methodology for tabletop scale batch reaction experiments of NaOH with $(NH_4)_2SO_4$ generating predictable low partial pressures of ammonia was designed to test the potential of biosolids (different barks from forestry wastes, oak wood, peats, coconut husk) as ammonia adsorbents and to compare their adsorption capacities with those of common adsorbents in the same conditions via adsorption isotherms data. The metal

analysis and lignin content demonstrated these materials were rich in lignin, calcium, and potassium, with little iron present, but metal content did not correlate with NH_3 adsorption capacity. A statistical comparison of the untreated vs. treated biosolids, showed superior adsorption capacity of the untreated biosolids, which also had significantly higher atomic H/C, O/C, and VM/FC than the treated equivalent. NH_3 adsorption capacities of untreated biosolids were of similar magnitude to those of many common NH_3 organic and inorganic adsorbents, albeit without the expected energy intensity of their production, indicating a promising valorisation route for wastes from forestry, peatlands, and agriculture residues. Potential uses as NH_3 adsorbents include maintaining air quality by plant management in hotspots of ammonia pollution (e.g., wastewater treatment and waste incineration plants), prevention of ammonia gas release by soil coverage following fertiliser application, fertiliser replacement, and mitigation of wastewater run-off. With further work at higher pressures, and on cyclic adsorption–desorption behaviour, industrial gas separation applications could also be investigated. This would also allow the identification of materials that could operate as adsorbents at larger scales under less ideal conditions. Rigorous assessment of the techno-economic-sustainability of the untreated lignin-rich biosolids compared to conventional NH_3 adsorbents could reveal environmental and societal benefits of the different intended applications of ammonia separation or capture.

Supplementary Materials: The following supporting information can be downloaded at: https://www.mdpi.com/article/10.3390/cleantechnol7020030/s1. Excel file containing the data for the article's graphs and tables.

Author Contributions: Conceptualisation, A.B.R. and D.C.; methodology, D.C., A.B.R. and V.D.; software, V.D. and D.C.; validation, V.D., D.C. and A.B.R.; formal analysis, V.D. and D.C.; investigation, D.C., V.D. and A.B.R.; resources, D.C. and A.B.R.; data curation, D.C. and V.D.; writing—original draft preparation, D.C. and V.D.; writing—review and editing, V.D., D.C. and A.B.R.; visualisation, V.D. and D.C.; supervision, A.B.R. and V.D.; project administration, D.C., A.B.R. and V.D.; funding acquisition, D.C. All authors have read and agreed to the published version of the manuscript.

Funding: This research was supported by the Engineering and Physical Sciences Research Council, grant number EP/L014912/1.

Institutional Review Board Statement: Not applicable.

Informed Consent Statement: Not applicable.

Data Availability Statement: All relevant data are provided in the Supplementary Materials.

Acknowledgments: Thank you to Adrian Cunliffe for aiding the elemental analysis portion of this research, and to Karine Alves Thorne for her assistance with the metals analysis and lignin determination.

Conflicts of Interest: The authors declare no conflicts of interest.

Abbreviations

The following abbreviations are used in this manuscript:

AAS	Atomic absorption spectroscopy
AC	Activated carbon
ADL	Acid detergent lignin
Ads	Adsorption
b	Temperature-dependent equilibrium constant
bc	Biochar
CH	Coconut husk
D	Polanyi adsorption potential
DF	Douglas-fir

DSC	Differential scanning calorimetry
E	Characteristic energy of the adsorbent–adsorbate system
Eq	Equilibrium
ESF	European silver fir
f	Fresh
FC	Fixed carbon
GF	Grand fir
H	Henry's constant
HW	Hot water washed
m	Mass
MC	Moisture content
n	Heterogeneity parameter
NC	Nootka cypress
NF	Noble fir
P	Pressure
q	Adsorption capacity
Q	Heat of adsorption
R	Ideal gas constant
S	Spent
SD	Standard deviation
TB	Treated biosolids
TGA	Thermogravimetric analysis
to	Toth heterogeneity factor
UB	Untreated biosolids
VM	Volatile matter
W	Molar mass
W0	Limiting pore volume of the adsorber bed material
x	Liquid phase mole fraction
y	Gas phase mole fraction
γ	Molar mass ratio
ρ	Density

References

1. ChemicalSafetyFacts. Ammonia. 2023. Available online: https://www.chemicalsafetyfacts.org/ (accessed on 18 July 2024).
2. Ryan, L. *Ammonia's Potential Role in a Low-Carbon Economy*; Congressional Research Service: Washington, DC, USA, 2022.
3. Fraser, B.A.D.; Phil, B.; David, F.; John, I.; Laura, T.M. *Ammonia: Zero-Carbon Fertiliser, Fuel and Energy Store*; The Royal Society: London, UK, 2020.
4. ChemAnalyst. Exploring Ammonia: Applications, Manufacturing Techniques, and Major Market Players! Available online: https://www.chemanalyst.com/ (accessed on 25 November 2024).
5. EasyChem. Industrial Uses of Ammonia. Available online: https://easychem.com.au/ (accessed on 18 July 2024).
6. Plautz, J. Piercing the haze. *Science* **2018**, *361*, 1060–1063. [CrossRef] [PubMed]
7. Ma, R.; Li, K.; Guo, Y.; Zhang, B.; Zhao, X.; Linder, S.; Guan, C.; Chen, G.; Gan, Y.; Meng, J. Publisher Correction: Mitigation potential of global ammonia emissions and related health impacts in the trade network. *Nat. Commun.* **2021**, *12*, 7084. [CrossRef] [PubMed]
8. Ren, S.; Huang, S.; Liu, B. Enhanced removal of ammonia nitrogen from rare earth wastewater by NaCl modified vermiculite: Performance and mechanism. *Chemosphere* **2022**, *302*, 134742. [CrossRef] [PubMed]
9. Chatain, M.; Chretien, E.; Crunaire, S.; Jantzem, E. Road Traffic and Its Influence on Urban Ammonia Concentrations (France). *Atmosphere* **2022**, *13*, 1032. [CrossRef]
10. Hansen, K.; Pryor, S.C.; Boegh, E.; Hornsby, K.E.; Jensen, B.; Sørensen, L.L. Background concentrations and fluxes of atmospheric ammonia over a deciduous forest. *Agric. For. Meteorol.* **2015**, *214–215*, 380–392. [CrossRef]
11. DEFRA. *ENV01—Emissions of Air Pollutants*; Department for Environment, Food & Rural Affairs: London, UK, 2024.
12. Saltworks. Ammonia Wastewater Treatment. Available online: https://www.saltworkstech.com/ (accessed on 18 July 2024).

13. Kesari, K.K.; Soni, R.; Jamal, Q.M.S.; Tripathi, P.; Lal, J.A.; Jha, N.K.; Siddiqui, M.H.; Kumar, P.; Tripathi, V.; Ruokolainen, J. Wastewater Treatment and Reuse: A Review of its Applications and Health Implications. *Water Air Soil. Pollut.* **2021**, *232*, 208. [CrossRef]
14. Gupta, V.K.; Saleh, T.A. Sorption of pollutants by porous carbon, carbon nanotubes and fullerene—An overview. *Environ. Sci. Pollut. Res.* **2013**, *20*, 2828–2843. [CrossRef]
15. Chen, M.; Li, J.; Zhang, J.; Ma, Y.; Dong, H.; Li, W.; Bekyarova, E.; Al-Hadeethi, Y.F.; Chen, L.; Hedhili, M.N.; et al. Evolution of cellulose acetate to monolayer graphene. *Carbon.* **2021**, *174*, 24–35. [CrossRef]
16. Fumoto, E.; Tago, T.; Masuda, T. Recovery of Ammonia and Ketones from Biomass Wastes. In *Progress in Biomass and Bioenergy Production*; Syed Shahid, S., Ed.; IntechOpen: Rijeka, Croatia, 2011; Volume 15.
17. Sáez-Guinoa, J.; García-Franco, E.; Llera-Sastresa, E.; Romeo, L.M. The effects of energy consumption of alumina production in the environmental impacts using life cycle assessment. *Int. J. Life Cycle Assess.* **2024**, *29*, 380–393. [CrossRef]
18. Parvulescu, A.-N.; Maurer, S. Toward sustainability in zeolite manufacturing: An industry perspective. *Front. Chem.* **2022**, *10*, 1050363. [CrossRef]
19. Brambila, C.; Boyd, P.; Keegan, A.; Sharma, P.; Vetter, C.; Ponnusamy, E.; Patwardhan, S.V. A Comparison of Environmental Impact of Various Silicas Using a Green Chemistry Evaluator. *ACS Sustain. Chem. Eng.* **2022**, *10*, 5288–5298. [CrossRef] [PubMed]
20. Sheraz, N.; Shah, A.; Haleem, A.; Iftikhar, F.J. Comprehensive assessment of carbon-, biomaterial- and inorganic-based adsorbents for the removal of the most hazardous heavy metal ions from wastewater. *RSC Adv.* **2024**, *14*, 11284–11310. [CrossRef] [PubMed]
21. Neme, I.; Gonfa, G.; Masi, C. Activated carbon from biomass precursors using phosphoric acid: A review. *Heliyon* **2022**, *8*, e11940. [CrossRef] [PubMed]
22. Zhang, Y.; Song, X.; Xu, Y.; Shen, H.; Kong, X.; Xu, H. Utilization of wheat bran for producing activated carbon with high specific surface area via NaOH activation using industrial furnace. *J. Clean. Prod.* **2019**, *210*, 366–375. [CrossRef]
23. Ajmani, A.; Patra, C.; Subbiah, S.; Narayanasamy, S. Packed bed column studies of hexavalent chromium adsorption by zinc chloride activated carbon synthesized from Phanera vahlii fruit biomass. *J. Environ. Chem. Eng.* **2020**, *8*, 103825. [CrossRef]
24. Luo, Y.; Li, D.; Chen, Y.; Sun, X.; Cao, Q.; Liu, X. The performance of phosphoric acid in the preparation of activated carbon-containing phosphorus species from rice husk residue. *J. Mater. Sci.* **2019**, *54*, 5008–5021. [CrossRef]
25. MacDermid-Watts, K.; Pradhan, R.; Dutta, A. Catalytic Hydrothermal Carbonization Treatment of Biomass for Enhanced Activated Carbon: A Review. *Waste Biomass Valorization* **2021**, *12*, 2171–2186. [CrossRef]
26. Jain, A.; Balasubramanian, R.; Srinivasan, M.P. Hydrothermal conversion of biomass waste to activated carbon with high porosity: A review. *Chem. Eng. J.* **2016**, *283*, 789–805. [CrossRef]
27. Othman, F.E.C.; Yusof, N.; Samitsu, S.; Abdullah, N.; Hamid, M.F.; Nagai, K.; Abidin, M.N.Z.; Azali, M.A.; Ismail, A.F.; Jaafar, J.; et al. Activated carbon nanofibers incorporated metal oxides for CO_2 adsorption: Effects of different type of metal oxides. *J. CO2 Util.* **2021**, *45*, 101434. [CrossRef]
28. Skoczko, I.; Guminski, R.; Bos, E.; Zglobicka, I. Impact of chemical activation on selected adsorption features of powdered activated carbon. *Desalin. Water Treat.* **2021**, *243*, 165–179. [CrossRef]
29. Udyani, K.; Purwaningsih, D.Y. Chemical and Physical Activation Using a Microwave to Increase the Ability of Activated Carbon to Adsorb Dye Waste. *J. Phys. Conf. Ser.* **2021**, *2117*, 012030. [CrossRef]
30. Song, L.; Xue, C.; Xia, H.; Qiu, S.; Sun, L.; Chen, H. Effects of Alkali Metal (Li, Na, and K) Incorporation in NH2–MIL125(Ti) on the Performance of CO_2 Adsorption. *Materials* **2019**, *12*, 844. [CrossRef] [PubMed]
31. Cardenas, C.; Sigot, L.; Vallières, C.; Marsteau, S.; Marchal, M.; Latifi, A.M. Ammonia capture by adsorption on doped and undoped activated carbon: Isotherm and breakthrough curve measurements. *Sep. Purif. Technol.* **2023**, *313*, 123454. [CrossRef]
32. Takaya, C.A.; Parmar, K.R.; Fletcher, L.A.; Ross, A.B. Biomass-Derived Carbonaceous Adsorbents for Trapping Ammonia. *Agriculture* **2019**, *9*, 16. [CrossRef]
33. Neiva, D.M.; Rencoret, J.; Marques, G.; Gutiérrez, A.; Gominho, J.; Pereira, H.; del Río, J.C. Lignin from Tree Barks: Chemical Structure and Valorization. *ChemSusChem* **2020**, *13*, 4537–4547. [CrossRef]
34. Şen, U.; Esteves, B.; Pereira, H. Pyrolysis and Extraction of Bark in a Biorefineries Context: A Critical Review. *Energies* **2023**, *16*, 4848. [CrossRef]
35. Catry, F.X.; Moreira, F.; Pausas, J.G.; Fernandes, P.M.; Rego, F.; Cardillo, E.; Curt, T. Cork Oak Vulnerability to Fire: The Role of Bark Harvesting, Tree Characteristics and Abiotic Factors. *PLoS ONE* **2012**, *7*, e39810. [CrossRef]
36. Pásztory, Z.; Mohácsiné, I.; Gorbacheva, G.; Börcsök, Z. The utilization of tree bark. *BioResources* **2016**, *11*, 7859–7888. [CrossRef]
37. Hammerton, J.; Joshi, L.R.; Ross, A.B.; Pariyar, B.; Lovett, J.C.; Shrestha, K.K.; Rijal, B.; Li, H.; Gasson, P.E. Characterisation of biomass resources in Nepal and assessment of potential for increased charcoal production. *J. Environ. Manag.* **2018**, *223*, 358–370. [CrossRef]
38. Fettweis, U.; Kuhl, J. Comparative Tests for the Purposes of a Crude Fibre Analysis Using Both the Official VDLUFA Method and FibreBag Technology (C. Gerhardt). *Analysis* **2010**, *3*, 804–810.

39. Quintana-Najera, J.; Blacker, A.J.; Fletcher, L.A.; Bray, D.G.; Ross, A.B. The Influence of Biochar Augmentation and Digestion Conditions on the Anaerobic Digestion of Water Hyacinth. *Energies* **2022**, *15*, 2524. [CrossRef]
40. Sun, Y.; Li, S.; Sun, R.; Yang, S.; Liu, X. Modified Dubinin–Astakhov Model for the Accurate Estimation of Supercritical Methane Sorption on Shales. *ACS Omega* **2020**, *5*, 16189–16199. [CrossRef] [PubMed]
41. NIST. Ammonia. Available online: https://webbook.nist.gov/ (accessed on 16 August 2024).
42. Ramirez, D.; Qi, S.; Rood, M.J.; Hay, K.J. Equilibrium and Heat of Adsorption for Organic Vapors and Activated Carbons. *Environ. Sci. Technol.* **2005**, *39*, 5864–5871. [CrossRef] [PubMed]
43. Haar, L.; Gallagher, J.S. Thermodynamic properties of ammonia. *J. Phys. Chem. Ref. Data* **1978**, *7*, 635–792. [CrossRef]
44. Serafin, J.; Dziejarski, B. Application of isotherms models and error functions in activated carbon CO_2 sorption processes. *Microporous Mesoporous Mater.* **2023**, *354*, 112513. [CrossRef]
45. Ferrer, V.; Flores, M.; Grandón, H.; Escalona, N.; Segura, C. Ammonia Removal in Activated Carbons Prepared from Olive Oil Industry Waste. *J. Braz. Chem. Soc.* **2023**, *34*, 287–301.
46. Rohatgi, A. *WebPlotDigitizer (version 4)*; Scientific Research Publishing Inc.: Irvine, CA, USA, 2024.
47. Tomczyk, A.; Sokołowska, Z.; Boguta, P. Biochar physicochemical properties: Pyrolysis temperature and feedstock kind effects. *Rev. Environ. Sci. Bio/Technol.* **2020**, *19*, 191–215. [CrossRef]
48. Bai, J.; Chen, X.; Shao, J.; Jia, C.; Wang, Q. Study of breakage of main covalent bonds during co-pyrolysis of oil shale and alkaline lignin by TG-FTIR integrated analysis. *J. Energy Inst.* **2019**, *92*, 512–522. [CrossRef]
49. Fromm, J. Wood formation of trees in relation to potassium and calcium nutrition. *Tree Physiol.* **2010**, *30*, 1140–1147. [CrossRef]
50. Helminen, J.; Helenius, J.; Paatero, E.; Turunen, I. Comparison of sorbents and isotherm models for NH3-gas separation by adsorption. *AIChE J.* **2000**, *46*, 1541–1555. [CrossRef]
51. Altun, A.; Kılıç, M. An investigation of the ammonia adsorption performance on different adsorbents for cooling applications. *Bulg. Chem. Commun.* **2018**, *50*, 45–52.
52. Chen, R.; Liu, J.; Dai, X. Adsorption equilibrium of ammonia and water on porous adsorbents at low pressure: Machine learning-based models. *J. Clean. Prod.* **2022**, *378*, 134351. [CrossRef]
53. Saha, D.; Deng, S. Characteristics of Ammonia Adsorption on Activated Alumina. *J. Chem. Eng. Data* **2010**, *55*, 5587–5593. [CrossRef]
54. Zhang, W.; Liu, F.; Kan, X.; Zheng, Y.; Zheng, A.; Liu, F.; Jiang, L. Developing ordered mesoporous silica superacids for high-precision adsorption and separation of ammonia. *Chem. Eng. J.* **2023**, *457*, 141263. [CrossRef]
55. Lucero, J.M.; Crawford, J.M.; Wolden, C.A.; Carreon, M.A. Tunability of ammonia adsorption over NaP zeolite. *Microporous Mesoporous Mater.* **2021**, *324*, 111288. [CrossRef]
56. Tang, S.; Wang, Z.; Liu, Z.; Zhang, Y.; Si, B. The Role of Biochar to Enhance Anaerobic Digestion: A Review. *J. Renew. Mater.* **2020**, *8*, 1033–1052. [CrossRef]
57. Munar-Florez, D.A.; Varón-Cardenas, D.A.; Ramírez-Contreras, N.E.; García-Núñez, J.A. Adsorption of ammonium and phosphates by biochar produced from oil palm shells: Effects of production conditions. *Results Chem.* **2021**, *3*, 100119. [CrossRef]
58. Fidel, R.B.; Laird, D.A.; Spokas, K.A. Sorption of ammonium and nitrate to biochars is electrostatic and pH-dependent. *Sci. Rep.* **2018**, *8*, 17627. [CrossRef]
59. Guo, X.; Tak, J.K.; Johnson, R.L. Ammonia removal from air stream and biogas by a H2SO4 impregnated adsorbent originating from waste wood-shavings and biosolids. *J. Hazard. Mater.* **2009**, *166*, 372–376. [CrossRef]
60. Rodrigues, C.C.; Moraes, D. Control of the Emission of Ammonia through Adsorption in a Fixed Bed of Activated Carbon. *Adsorpt. Sci. Technol.* **2002**, *20*, 1013–1022. [CrossRef]
61. Ngo, T.; Khudur, L.S.; Hakeem, I.G.; Shah, K.; Surapaneni, A.; Ball, A.S. Wood Biochar Enhances the Valorisation of the Anaerobic Digestion of Chicken Manure. *Clean. Technol.* **2022**, *4*, 420–439. [CrossRef]
62. Lv, Y.; Zhang, L.; Wang, Y. Simultaneously improving surface area and hydrophilicity of biomass activated carbon for achieving superior desalination performance in CDI. *Desalin. Water Treat.* **2024**, *318*, 100318. [CrossRef]
63. Pérez-Botella, E.; Valencia, S.; Rey, F. Zeolites in Adsorption Processes: State of the Art and Future Prospects. *Chem. Rev.* **2022**, *122*, 17647–17695. [CrossRef] [PubMed]
64. Wójtowicz, M.A.; Cosgrove, J.E.; Serio, M.A.; Wilburn, M.S. Adsorption of Ammonia on Regenerable Carbon Sorbents. In Proceedings of the 45th International Conference on Environmental Systems, Bellevue, WA, USA, 13–17 July 2015.
65. Abdullahi, T.; Harun, Z.; Othman, M.H.D. A review on sustainable synthesis of zeolite from kaolinite resources via hydrothermal process. *Adv. Powder Technol.* **2017**, *28*, 1827–1840. [CrossRef]
66. Dehghani, M.H.; Ahmadi, S.; Ghosh, S.; Othmani, A.; Osagie, C.; Meskini, M.; AlKafaas, S.S.; Malloum, A.; Khanday, W.A.; Jacob, A.O.; et al. Recent advances on sustainable adsorbents for the remediation of noxious pollutants from water and wastewater: A critical review. *Arab. J. Chem.* **2023**, *16*, 105303. [CrossRef]

67. Zhou, G.-T.; Wang, Y.-L.; Qi, T.-G.; Zhou, Q.-s.; Liu, G.-H.; Peng, Z.-h.; Li, X.-B. Toward sustainable green alumina production: A critical review on process discharge reduction from gibbsitic bauxite and large-scale applications of red mud. *J. Environ. Chem. Eng.* **2023**, *11*, 109433. [CrossRef]
68. Zhou, G.-T.; Wang, Y.-L.; Zhang, Y.-G.; Qi, T.-G.; Zhou, Q.-S.; Liu, G.-H.; Peng, Z.-H.; Li, X.-B. A clean two-stage Bayer process for achieving near-zero waste discharge from high-iron gibbsitic bauxite. *J. Clean. Prod.* **2023**, *405*, 136991. [CrossRef]
69. Curdts, B.; Pflitsch, C.; Pasel, C.; Helmich, M.; Bathen, D.; Atakan, B. Novel silica-based adsorbents with activated carbon structure. *Microporous Mesoporous Mater.* **2015**, *210*, 202–205. [CrossRef]
70. Taiye, M.A.; Hafida, W.; Kong, F.; Zhou, C. A review of the use of rice husk silica as a sustainable alternative to traditional silica sources in various applications. *Environ. Prog. Sustain. Energy* **2024**, *43*, e14451. [CrossRef]
71. Hu, D.; Cao, G.; Du, M.; Huang, J.; Zhao, J.; Li, C.; Fang, Y. Insight into the biomass pyrolysis volatiles reaction with an iron-based oxygen carrier in a two-stage fixed-bed reactor. *Chem. Eng. J.* **2023**, *465*, 142860. [CrossRef]
72. Na-Lampang, C.; Assawasaengrat, P.; Phumjan, L.; Narkrugsa, W.; Sriprom, P. Optimizing Ammonia Adsorption Using Activated Carbon from Tamarind Pulp. *J. Jpn. Inst. Energy* **2021**, *100*, 288–293. [CrossRef]
73. Parihar, A.; Sripada, P.; Bambery, K.; Garnier, G.; Bhattacharya, S. Investigation of functional group changes in biomass during slow pyrolysis using synchrotron based infra-red microspectroscopy and thermogravimetry-infra-red spectroscopy. *J. Anal. Appl. Pyrolysis* **2017**, *127*, 394–401. [CrossRef]
74. El-Sayed, S.A.; Khass, T.M.; Mostafa, M.E. Thermal degradation behaviour and chemical kinetic characteristics of biomass pyrolysis using TG/DTG/DTA techniques. *Biomass Convers. Biorefinery* **2024**, *14*, 17779–17803. [CrossRef]
75. Le, D.; Nielsen, A.; Sørensen, H.; Meyer, A. Characterisation of Authentic Lignin Biorefinery Samples by Fourier Transform Infrared Spectroscopy and Determination of the Chemical Formula for Lignin. *BioEnergy Res.* **2017**, *10*. [CrossRef]
76. Wu, L.; Chowdhury, A.; Zhou, Z.; Chen, K.; Wang, W.; Niu, J. Precision Cellulose from Living Cationic Polymerization of Glucose 1,2,4-Orthopivalates. *J. Am. Chem. Soc.* **2024**, *146*, 7963–7970. [CrossRef]
77. Kaur, R.; Sharma, M. Cereal polysaccharides as sources of functional ingredient for reformulation of meat products: A review. *J. Funct. Foods* **2019**, *62*, 103527. [CrossRef]